Cytotoxicity of the soluble and insoluble fractions of atmospheric fine particulate matter

Ling Liu [1], *Qiuhua Zhou* [1], *Xuezhi Yang* [1], *Gang Li* [2], *Jingzhu Zhang* [1], *Xuehua Zhou* [1], *Wei Jiang* [1,*]

[1] Environment Research Institute, Shandong University, Qingdao 266237, China
[2] State Key Laboratory of Environmental Chemistry and Ecotoxicology, Research Center for Eco-Environmental Sciences, Chinese Academy of Sciences, Beijing 100085, China

ARTICLE INFO

ABSTRACT

Inhaled atmospheric fine particulate matter (PM$_{2.5}$) includes soluble and insoluble fractions, and each fraction can interact with cells and cause adverse effects. PM$_{2.5}$ samples were collected in Jinan, China, and the soluble and insoluble fractions were separated. According to physiochemical characterization, the soluble fraction mainly contains water-soluble ions and organic acids, and the insoluble fraction mainly contains kaolinite, calcium carbonate and some organic carbon. The interaction between PM$_{2.5}$ and model cell membranes was examined with a quartz crystal microbalance with dissipation (QCM-D) to quantify PM$_{2.5}$ attachment on membranes and membrane disruption. The cytotoxicity of the total PM$_{2.5}$ and the soluble and insoluble fractions, was investigated. Negatively charged PM$_{2.5}$ can adhere to the positively charged membranes and disrupt them. PM$_{2.5}$ also adheres to negatively charged membranes but does not cause membrane rupture. Therefore, electrostatic repulsion does not prevent PM$_{2.5}$ attachment, but electrostatic attraction induces remarkable membrane rupture. The human lung epithelial cell line A549 was used for cytotoxicity assessment. The detected membrane leakage, cellular swelling and blebbing indicated a cell necrosis process. Moreover, the insoluble PM$_{2.5}$ fraction caused a higher cell mortality and more serious cell membrane damage than the soluble fraction. The levels of reactive oxygen species (ROS) enhanced by the two fractions were not significantly different. The findings provide more information to better understand the mechanism of PM$_{2.5}$ cytotoxicity and the effect of PM$_{2.5}$ solubility on cytotoxicity.

© 2020 The Research Center for Eco-Environmental Sciences, Chinese Academy of Sciences. Published by Elsevier B.V.

Introduction

Fine particulate matter (PM$_{2.5}$, aerodynamic diameter ≤ 2.5 μm) is considered an indicator of air pollution and is associated with a series of adverse health effects (Zhuang et al., 2014; Feng et al., 2016; Kioumourtzoglou et al., 2016). PM$_{2.5}$ can cause inflammation, oxidative damage, and DNA damage, which trigger pulmonary, cardiovascular and nervous system diseases and even cancer (Indo et al., 2007; Gualtieri et al., 2011; Ray et al., 2012; Deng et al., 2013). The main cytotoxicity mechanisms of PM$_{2.5}$ are cell particle interaction and production of excess reactive oxygen species (ROS), which can upset the dynamic balance of intracellular oxides and antioxidants (Wang et al., 2013b; Zou et al., 2016).

$PM_{2.5}$ is composed of an inert carbonaceous core covered by sulfate, nitrate, organic chemicals, metals, and crustal elements (Zou et al., 2016). Additional organic pollutants, bacteria, viruses and toxic heavy metals adsorbed on particulate matter (PM), can enhance its toxicity (Cao et al., 2014). $PM_{2.5}$ can be transported deeply into the lungs to reach alveoli. The fine particles can penetrate multilayer barriers of the respiratory system (even the blood-air barrier), arrive at remote organs, and affect human health (Calderón-Garcidueñas et al., 2008; Block and Calderón-Garcidueñas, 2009).

Alveoli are important $PM_{2.5}$ deposition site. Thus, alveolar epithelial cells are commonly used to study the cytotoxicity of $PM_{2.5}$ (Thron, 1996; Kampa and Castanas, 2008). Cells are surrounded by extracellular fluid, such as blood plasma, interstitial fluid and lymph. $PM_{2.5}$ must penetrate the extracellular fluid before contacting human cells; hence, the soluble and insoluble $PM_{2.5}$ fractions will be separated via dissolution. The different cytotoxicities of the soluble and insoluble $PM_{2.5}$ fractions were investigated to a limited extent in previous studies. Oxidative stress is a widely accepted mechanism in $PM_{2.5}$-mediated cytotoxicity (Yan et al., 2016). The soluble $PM_{2.5}$ fraction was reported to contribute the majority of the macrophage ROS activity per volume of sampled air (Wang et al., 2013b), but some of the insoluble species have an intrinsically higher ROS activity and generate more ROS with increasing exposure time (Wang et al., 2013b; Zou et al., 2016). Oxidative stress can lead to the release of inflammatory mediators such as interleukin-8 (IL-8) and tumor necrosis factor alpha (TNF-a) (Yan et al., 2016). Oxidative stress and inflammation are significant molecular mechanisms of $PM_{2.5}$-mediated cytotoxicity (Valavanidis et al., 2008; Yan et al., 2016). Both the soluble and insoluble fractions have been reported to induce IL-8 expression in human bronchial epithelial and macrophage-like cells (Yan et al., 2016), and the insoluble fractions play a major role in TNF-a expression in human alveolar macrophages (Soukup and Becker, 2001). Oxidative stress also causes lipid peroxidation in cell membranes. Serious cell membrane disruption induced by the insoluble $PM_{2.5}$ fraction was detected via the lactate dehydrogenase (LDH) assay and microscopic observation (Geng et al., 2006; Gualtieri et al., 2009; Zou et al., 2016; Vuong et al., 2017). However, it is difficult to assess whether the membrane damage is induced by the physical contact of $PM_{2.5}$ or whether it occurs as a phenomenon in the process of cell necrosis caused by the internalized $PM_{2.5}$. Although many cytotoxicity studies of soluble and insoluble $PM_{2.5}$ fractions have been conducted, the knowledge about how the two fractions interact with the cells and cause different effects is still limited. Therefore, the role and mechanism of the soluble and insoluble $PM_{2.5}$ fractions in cytotoxicity need further investigation.

The purpose of this research is to investigate the cytotoxicity of the total $PM_{2.5}$ and the soluble and insoluble $PM_{2.5}$ fractions and to examine the toxic mechanisms of different $PM_{2.5}$ components. $PM_{2.5}$ was collected at an urban site near central Jinan, China. The soluble and insoluble fractions were separated by centrifugation. The attachment of $PM_{2.5}$ on membranes and physical membrane ruptures were monitored using model cell membranes on a quartz crystal microbalance with dissipation (QCM-D). A549 cell lines (human alveolar type II epithelial cells) were exposed to the total $PM_{2.5}$ and the soluble and insoluble $PM_{2.5}$ fractions to investigate cell viability, cell membrane leakage, and the induced ROS generation.

1.   Materials and methods

1.1.   Materials and chemical agents

Phospholipids 1,2-dioleoyl-sn-glycero-3-phosphocholine (DOPC), 1,2-dioleoyl-sn- glycero-3-[phosphor-rac-(1-glycerol)] (sodium salt) (DOPG), and 1,2-dipalmitoyl-3-trimethylammonium-propane (chloride salt) (16:0 TAP) were purchased from Avanti Polar Lipids (Alabaster, AL, USA). Tris-(hydroxymethyl)-aminomethane (Tris) was purchased from Amresco (Solon, OH, USA) as a buffer in the QCM-D experiments. The 3-(4,5-dimethylthiazoyl-2-thiazoyl)-2,5-diphenyl-2-H-tetrazolium bromide (MTT) cell proliferation and cytotoxicity and lactate dehydrogenase (LDH) assay kits were purchased from Beyotime (Beijing, China). Dimethylsulfoxide (DMSO) solution and ROS assay kits were provided by Solarbio (Beijing, China). RPMI 1640 medium modified, 0.25% (W/V) trypsin solution, fetal bovine serum (FBS) and penicillin-streptomycin solution were purchased from HyClone (USA) for cell culture.

1.2. $PM_{2.5}$ collection and preparation of the soluble and insoluble fractions

$PM_{2.5}$ samples were collected from December 2016 to March 2017 at Shandong University (36.67°N, 117.05°E) in Jinan, China. Surrounded by residential and commercial buildings and without major stationary sources, this site is representative of the residential areas in Jinan City. $PM_{2.5}$ samples were collected on polycarbonate filters (90-mm diameter, 0.4 μm HTTP, Merck Millipore Ltd., Germany) by a medium-volume $PM_{2.5}$ sampler at a flow rate of 100 L/min. Simultaneously, $PM_{2.5}$ samples were also collected on quartz filters for compositional analysis. Before and after sampling, the filters were equilibrated for 24 hr at (20 ± 1)°C and a relative humidity of $50\% \pm 5\%$ and then weighed with an analytical balance (Sartorius, Germany; detection limit: 0.001 mg). To eliminate organic compounds, the quartz filters were baked at 600°C for 2 hr before weighing. The collected mass on each filter was quantified through the subtraction method. The polycarbonate and quartz filters were stored in a refrigerator at −20°C after sampling. To separate $PM_{2.5}$ from the polycarbonate filters, the filters containing samples were sonicated for 3 hr to disperse $PM_{2.5}$ into deionized (DI) water (18.25 MΩ cm), and then the intact polycarbonate filter was removed from the suspension. The $PM_{2.5}$ in DI water was freeze dried, and an accurate $PM_{2.5}$ mass was obtained. The freeze-dried $PM_{2.5}$ sample resuspended in DI water to prepare a 2 mg/mL suspension and was divided into two equal aliquots. One aliquot represented the total $PM_{2.5}$. The other aliquot was centrifuged at 3000 r/min for 1 hr. The supernatant was collected as the soluble $PM_{2.5}$ fraction. The remaining residue was the insoluble $PM_{2.5}$ fraction. The collected soluble and insoluble fractions (freeze dried) accounted for

approximately 42% and 46%, respectively, of the total $PM_{2.5}$ (mass). The total $PM_{2.5}$ and the soluble and insoluble $PM_{2.5}$ fractions were diluted in cell culture medium and sterilized under ultraviolet light for 2 hr for the cytotoxicity experiments. For the other experiments, the total $PM_{2.5}$ and the soluble and insoluble $PM_{2.5}$ fractions were diluted in DI water, and the pH was adjusted to 7.0 ± 0.2; moreover, the solutions were sonicated for 30 min (40 kHz).

1.3.　Characterization of the $PM_{2.5}$ samples

To investigate the major functional groups in the total $PM_{2.5}$ and the soluble and insoluble $PM_{2.5}$ fractions, the freeze-dried samples were analyzed with a Fourier transform infrared spectrometer coupled with an attenuated total reflectance (ATR-FTIR) spectrometer (VERTEX 70, Bruker, Germany). The samples were pressed against the ATR crystal by a regulated pressure tower to collect more than 50 scans at a spectral resolution of 4.0 cm^{-1} (Anıl et al., 2014). Three-dimensional fluorescence spectra of the 200 mg/L soluble $PM_{2.5}$ fraction were obtained with a fluorescence spectrophotometer (F-7000, Hitachi, Japan) to analyze the soluble organics (Duarte et al., 2004). The diameter and zeta potential of the total $PM_{2.5}$ in DI water (20 mg/L) were measured after 20 min of sonication using a Malvern Zetasizer (Nano ZS90, Malvern Instrument, UK). The concentrations of fifteen elements (Si, Ca, S, Cl, Fe, Al, K, Na, Mg, Ti, P, Mn, Cr, Cu, and Zn) in the collected $PM_{2.5}$ samples were determined directly on the polycarbonate filters by X-ray fluorescence (XRF) spectroscopy (ARL Perform'X 4200, Thermo Fisher, Switzerland) (Zhang et al., 2018). For organic carbon (OC) and elemental carbon (EC) analysis, a 1.5 cm^2 quartz filter section with the collected $PM_{2.5}$ was placed onto an instrument tray, and then the tray was pushed into the instrument. The OC/EC content in $PM_{2.5}$ was detected with a thermal-optical transmission (TOT) carbon analyzer (Sunset Laboratory Inc., USA) operated with the NIOSH870 thermal protocol (Panteliadis et al., 2015). To analyze the organic acids and water-soluble ions, the extracted 1.5 cm^2 quartz filter with the collected $PM_{2.5}$ was sonicated in 20 mL ultra-pure water for 20 min. The filter was then removed, and the suspension was filtered through a 0.22 μm PES (polyethersulfone resins) filter to obtain the filtrate (Nie et al., 2010). The concentrations of organic acids (acetic, formic, lactic, methane sulfonic, and oxalic acids) were determined using ion chromatography (IC) (Dionex 2500, USA) (Karthikeyan and Balasubramanian, 2006). The water-soluble NH_4^+, Na^+, K^+, Mg^{2+} and Ca^{2+} were measured via ion chromatography (Dionex 2500, USA) and the water-soluble Cl^-, SO_4^{2-} and NO_3^- were measured by ion chromatography (Dionex 90, USA) (Zou et al., 2016).

1.4.　Preparation of the SUVs for the QCM-D experiments

A QCM-D (Q-Sense E4, Västra Frölunda, Sweden) was used to examine the interaction between $PM_{2.5}$ and the lipid membranes. The quartz crystal microbalance (QCM) sensor (Au) was coated with a layer of small unilamellar vesicles (SUVs) to simulate cell membranes (Keller and Kasemo, 1998). The SUVs were prepared by the extrusion method, containing 10% (by mass) positively charged 16:0 TAP or negatively charged DOPG (Cho et al., 2010; Zhang et al., 2019). The 20 mg/L $PM_{2.5}$ solution

was injected for 1 hr to study the interaction between $PM_{2.5}$ and the SUVs. $PM_{2.5}$ deposition was detected by assessing the oscillation frequency shift (Δf) and energy dissipation shift (ΔD) of the Au crystal sensor on each module of the QCM-D (Yousefi and Tufenkji, 2016). The Δf and ΔD values are associated with the mass change (Δm) and viscoelasticity of cell membranes, respectively (Rodahl et al., 1997; Zhang et al., 2019). Hence, $PM_{2.5}$ adhesion on lipid membranes and SUV disruption were revealed by the changes in Δf and ΔD.

1.5.　Cell culture and treatments

A human lung epithelial cell line (A549) was obtained from the cell bank of the Chinese Academy of Sciences. A549 cells were cultured using PRIM-1640 medium with 10% FBS and 1% penicillin/streptomycin (Gibco, Invitrogen, Merelbeke,

Table 1 – Concentration of chemical species in the collected $PM_{2.5}$ samples.

Species	Mean concentration in air (μg/m^3)	Concentration in the total collected mass (μg/mg)
Total mass	207.88 ± 117.24	—
Carbon contents		
EC	2.77 ± 1.78	13.32
OC	24.96 ± 13.44	120.07
Organic acids		
Acetic	0.43 ± 0.20	2.07
Formic	0.21 ± 0.08	1.01
Lactic	0.22 ± 0.10	1.06
Methane sulfonic	0.16 ± 0.10	0.77
Oxalic acid	0.42 ± 0.18	2.02
Water-soluble ions		
Ca^{2+}	1.21 ± 0.76	5.82
Cl^-	5.72 ± 4.61	27.52
K^+	1.99 ± 1.46	9.57
Mg^{2+}	0.19 ± 0.20	0.91
NH_4^+	15.30 ± 10.46	73.6
NO_3^-	19.68 ± 13.44	94.67
Na^+	0.77 ± 0.42	3.7
SO_4^{2-}	26.96 ± 26.69	129.69
Elements		
Al	—	10.1 ± 0.50
Ca	—	17.1 ± 0.99
Cl	—	41.2 ± 1.40
Cr	—	1.74 ± 0.49
Cu	—	0.87–1.44
Fe	—	14.6 ± 0.98
K	—	20.1 ± 0.68
Mg	—	3.14 ± 0.25
Mn	—	0.40–0.70
Na	—	4.21 ± 0.39
P	—	0.70 ± 0.05
S	—	83.1 ± 0.50
Si	—	32.0 ± 0.82
Ti	—	0.74 ± 0.15
Zn	—	0.64–3.79

$PM_{2.5}$: Fine particulate matter with aerodynamic diameter ≤ 2.5 μm. EC: elemental carbon; OC: organic carbon. "-" means no number here.

Belgium) and incubated with 5% CO_2 at 37°C. Cells were harvested with 0.25% trypsin at 85% confluence and then subcultured in well plates for the next cytotoxicity experiments.

1.6. MTT and LDH assays

Cell viability was evaluated by testing the activity of dehydrogenase in mitochondria using the MTT cell proliferation and cytotoxicity assay kit. In this assay, the A549 cells were cultured in a 96-well plate at a density of approximately 1×10^4 cells per well and incubated at 37°C for 24 hr. Then, the cells were treated with the total $PM_{2.5}$ and soluble and insoluble $PM_{2.5}$ fractions at concentrations of 0, 50, 100, and 200 mg/L for 24 hr. Simultaneously, the cells cultured in the absence of $PM_{2.5}$ were set as control samples. After 24 hr, 10 μL MTT (5 mg/mL) was added and coincubated for 4 hr. Then, 100 μL DMSO was added and oscillated at low speed at 37°C to dissolve any formazan crystals. The optical density (OD) was measured by a microplate reader at 570 nm.

Cell membrane damage was estimated using an LDH assay kit. The A549 cells were treated with $PM_{2.5}$ as in the MTT assay. After $PM_{2.5}$ treatment, the 96-well plate was centrifuged at 80 r/min for 5 min. Then, 120 μL of the supernatant was collected from each well and added to a new 96-well plate. The LDH activity measurement was conducted according to the instructions in the LDH assay kit. The optical density (OD) was measured by a microplate reader at 490 nm.
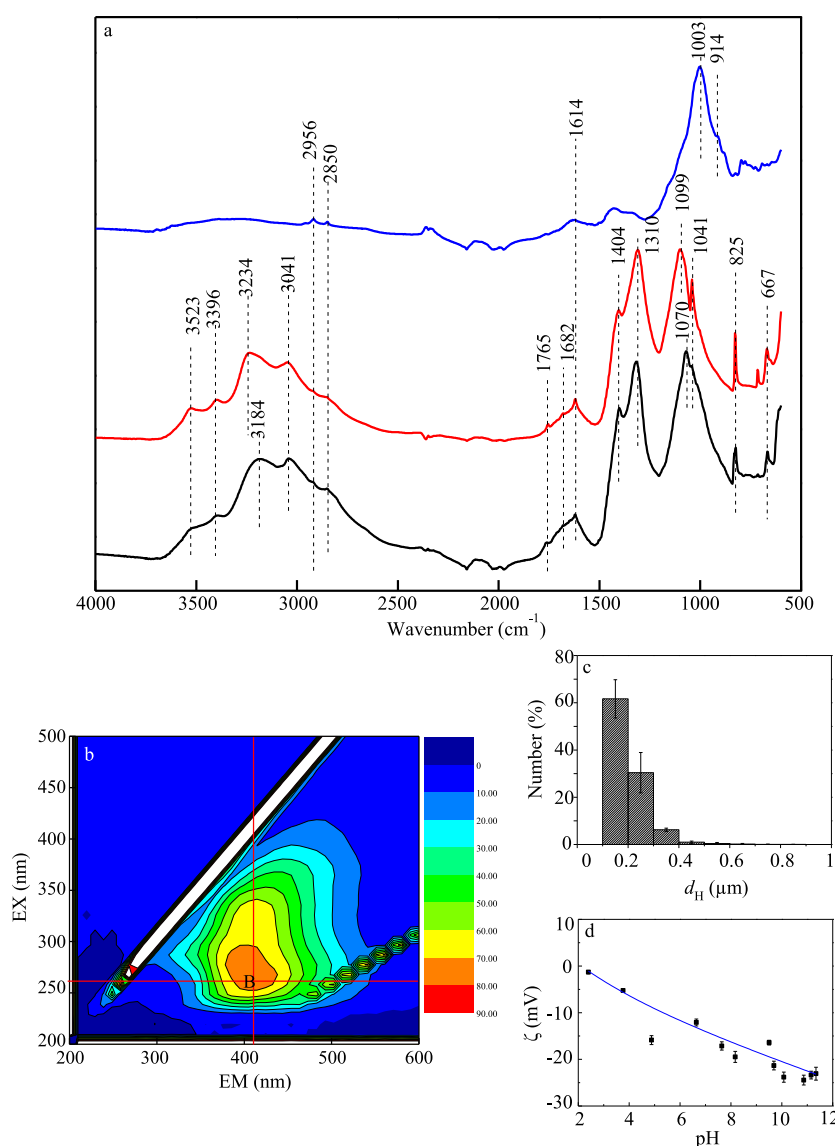

Fig. 1 − The characteristics of the total fine particulate matter ($PM_{2.5}$, aerodynamic diameter ≤ 2.5 μm), insoluble and soluble fractions. (a) The infrared spectrum of the total $PM_{2.5}$ (black line), insoluble fraction (red line) and soluble fraction (blue line); (b) The 3-D fluorescence spectra of the soluble fraction; (c) The size distribution of 20 mg/L $PM_{2.5}$ in deionized (DI) water; (d) The zeta potential of 20 mg/L $PM_{2.5}$ at different pH. Error bars represent standard deviations for three replicates. EX: excitation wavelength, EM: emission wavelength, d_H: hydrodynamic diameter.

1.7. ROS assay

The increase in ROS level in the A549 cells after $PM_{2.5}$ treatment was calculated based on the fluorescence intensity. To determine the effect of the $PM_{2.5}$ concentration on the intracellular ROS, the A549 cells were treated with total $PM_{2.5}$ (0, 50, 100, and 200 mg/L) and 200 mg/L soluble and insoluble $PM_{2.5}$ fractions for 48 hr. Thereafter, the cells were incubated with 10 μmol/L 2′,7′-dichlorofluorescein diacetate (DCFH-DA) for 20 min, and then the cells were rinsed three times with serum-free medium to remove any remaining DCFH-DA. The cells cultured without $PM_{2.5}$ were set as control groups. The cells treated with rosup solution (50 mg/mL H_2O_2) were considered as positive controls because H_2O_2 was able to oxidize 2′,7′-dichlorofluorescein (DCFH) into fluorescent 2′,7′-chlorofluorescein (DCF). The fluorescence intensity was quantified at an excitation/emission wavelength of 488/525 nm using a fluorescence microplate reader (Varioskan LUX, Thermo Fisher, USA). The relative fluorescence intensity was normalized by the fluorescence intensity of the control group. Bright-field and fluorescence images were obtained with an inverted fluorescence microscope.

1.8. Statistical analysis

All statistical analyses were performed with SigmaPlot 12.5 software (Systat Software Inc., San Jose, USA). Experimental results were expressed as the mean ± standard deviation (S.D.). Statistical differences of experimental groups compared to control groups were tested with one-way ANOVA via the Tukey test. The differences between two experimental groups (the soluble and insoluble fractions in this study) were tested with Two-tailed Student's t test. Statistical differences were considered to be significant at the 95% level ($p < 0.05$).

2. Results and discussion

2.1. The physicochemical properties of $PM_{2.5}$

The average daily $PM_{2.5}$ concentration was 207.88 μg/m^3 in the sample collection period. This indicated serious fine particulate matter pollution according to the National Ambient Air Quality Standard (35 μg/m^3). The average mass concentrations of carbon, organic acids, water-soluble ions and the fifteen elements in $PM_{2.5}$ ware listed in Table 1. The OC and EC contents contributed 13.3% of the $PM_{2.5}$ mass. Approximately half of the OC fraction was soluble in water, while EC was completely insoluble (Gualtieri et al., 2009). The mass of the detected organic acid species was very low in the total collected $PM_{2.5}$. Acetic acid (2.07 μg/mg) and oxalic acid (2.02 μg/mg) concentrations were higher than those of the other organic acids. Cl^-, SO_4^{2-}, NO_3^-, NH_4^+ and K^+ were the dominant water-soluble ions and contributed 33.5% of the $PM_{2.5}$ mass. S, Cl and Si were the abundant nonmetallic elements and their mass concentrations were 83.1, 41.2 and 32.0 μg/mg, respectively. K, Ca, Fe and Al were also high-content elements (>10 μg/mg) in $PM_{2.5}$. The hydrodynamic diameter of $PM_{2.5}$ revealed that more than 90% (by number) of the diameter of the particles was distributed between 100 and
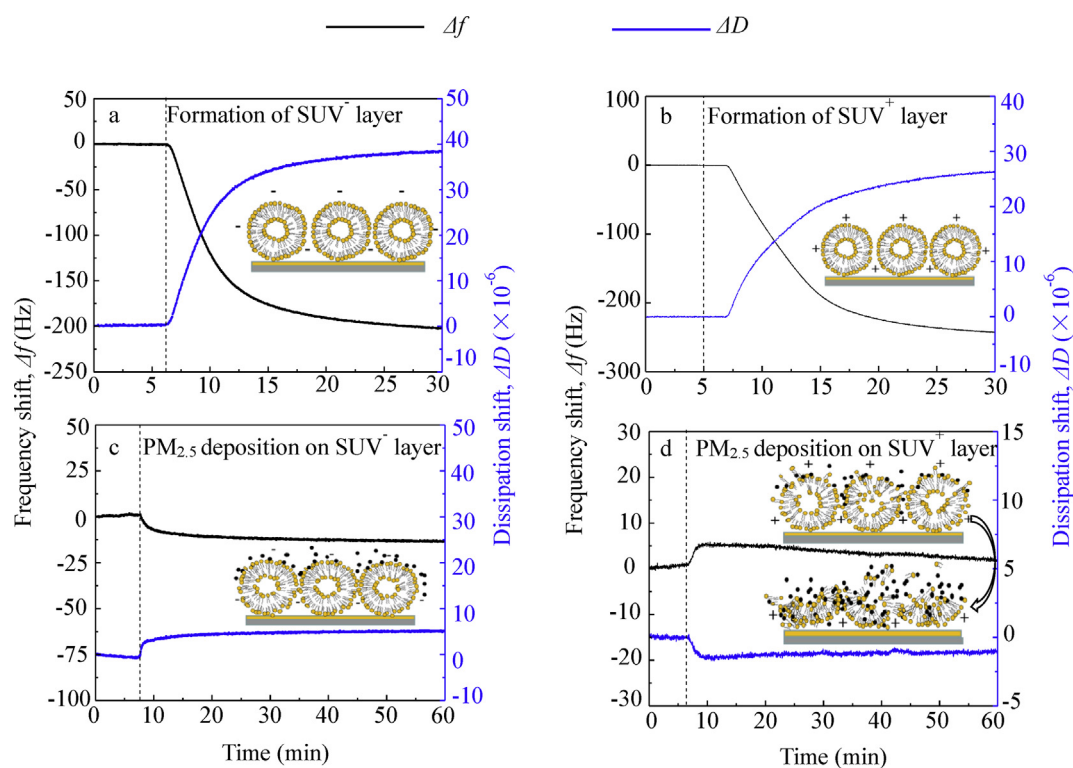

Fig. 2 – The diagram shows the formation process of a layer of small unilamellar vesicles (SUVs) on the Au sensor (a, b) and deposition kinetics of $PM_{2.5}$ on SUVs (c, d). $PM_{2.5}$ (20 mg/L) was injected at 5 min after the baseline is stable. Black lines: Δf (Hz); Blue lines: ΔD ($\times 10^{-6}$). The experiment was repeated at least three times.

1000 nm. The PM$_{2.5}$ fraction in the 100–200 nm ranged formed the highest column, and the average particle diameter was 276.94 nm (Fig. 1c). The zeta potential of the 20 mg/L PM$_{2.5}$ solution at different pH values is shown in Fig. 1d. PM$_{2.5}$ was negatively charged in the pH range from 2 to 12, and its zeta potential was approximately −15 mV at a pH of 7.

The insoluble and soluble fractions in the collected PM$_{2.5}$ samples were separated and scanned with the ATR-FTIR in addition to the whole PM$_{2.5}$ sample (Fig. 1a). Among the spectra of the PM$_{2.5}$ samples, the bands at 3523 and 3396 cm^{-1} were assigned to O–H stretching of phenol, hydroxyl and carboxyl groups (Duarte et al., 2007; Anıl et al., 2014), which remarkably decreased in the insoluble fraction. The bands at approximately 3234, 3184 and 3041 cm^{-1} in the whole and soluble PM$_{2.5}$ samples were attributed to N–H stretching vibrations of ammonium (Shaka and Saliba, 2004; Anıl et al., 2014; Zhou et al., 2016). Both O–H and N–H stretching vibrations diminished in the insoluble fraction. The weak absorptions at 2956 and 2850 cm^{-1} were due to C–H stretching vibrations of CH$_3$ and CH$_2$ in hydrocarbons (Zhu et al., 2001; Shaka and Saliba, 2004; Duarte et al., 2007). The bands at 1765 and 1682 cm^{-1} belonged to carbonyl (C=O) stretching of carboxylic acids (Allen et al., 1994; Zhu et al., 2001; Ofner et al., 2011). The band at 1614 cm^{-1} was assigned to organonitrate (Shaka and Saliba, 2004), which decreased in the insoluble fraction. The adsorption at 1404 cm^{-1} was assigned to NH$_4$ deformation (Allen et al., 1994). The band at 1310 cm^{-1} was assigned to NO$_3^-$ (Maria et al., 2002), and the band at 1099 cm^{-1}

in the soluble fraction was attributed to the SO$_4^{2-}$ deformation (Shaka and Saliba, 2004). The three bands mentioned above almost disappeared in the insoluble fraction (Fig. 1a). The adsorption at 1070 cm^{-1} in the insoluble fraction belongs to the aliphatic C–O stretch vibration of aliphatic-aromatic ethers (Zhu et al., 2001). The strong absorption peak at 1041 cm^{-1} was due to silicate, which occurred in the insoluble fraction. The peaks centered around 1003 cm^{-1} and 914 cm^{-1} were caused by Si–O stretching and Al–OH vibrations in kaolinite, respectively (Ravisankar et al., 2010; Anıl et al., 2014; Zhou et al., 2016). The absorption at 825 cm^{-1} in the total PM$_{2.5}$ sample and the soluble fraction was due to the nitrate group (Allen et al., 1994).

The three-dimensional excitation-emission matrix of the fluorescence spectrum of the soluble PM$_{2.5}$ fraction was obtained (Fig. 1b). The highest fluorescence intensity of the soluble fraction was located at an excitation/emission wavelength (Ex/Em) of 260/410 nm (site B) (Fig. 1b). A previous study found that these excitation ranges (250–260 nm) and emission (380–480 nm) characterized humic-like substances (Leenheer and Croué, 2003; Graber and Rudich, 2006). Due to the location in this range, peak B of the soluble PM$_{2.5}$ fraction was assigned to humic-like substances. Quinone moieties in the humic-like substances had been confirmed to contribute significantly to fluorescence (Klapper et al., 2002). Humic-like substances accounted for a large proportion (30%–80%) of the water-soluble organic matter in PM$_{2.5}$ (Ma et al., 2018), and the carbon mass in the humic-like substances accounted for 32%–43% of the water-soluble organic carbon in the airborne particulate matter (Voliotis et al., 2017), which contained polycyclic ring structures and polar functional groups. The humic-like substances in PM$_{2.5}$ could disturb the redox equilibrium in lung cells and subsequently cause oxidative stress (Ma et al., 2018).

From the infrared (IR) spectra (Fig. 1a) and the three-dimensional fluorescence spectra (Fig. 1b), the soluble PM$_{2.5}$ fraction contained NH$_4^+$, SO$_4^{2-}$, NO$_3^-$, SiO$_3^{2-}$, organic acids, organic carbon, quinone moieties, oxygenated phenolic and aromatic compounds, organonitrates, and hydroxyl, carboxyl and aliphatic groups. The insoluble fraction contained kaolinite, aliphatic carbons, and carboxyl and hydroxyl groups. Understanding the components and properties of the soluble and insoluble PM$_{2.5}$ fractions is helpful in determining to find out the mechanism of toxicity.

2.2. The interaction between PM$_{2.5}$ and model membranes

The layer of SUVs on the Au sensor was used to monitor the combined mass changes due to PM$_{2.5}$ adhesion and vesicle rupture. When 0.1 mg/mL SUVs was injected into the QCM chamber, a layer of negatively or positively charged SUVs formed on the sensor surface (Fig. 2a and b). The Δf and ΔD changes were caused by the mass and membrane viscoelasticity changes on the Au sensor. During SUV layer formation, Δf decreased because SUVs were gradually deposited on the sensor. Then, Δf stabilized, which indicated that only one layer of SUVs had formed on the Au sensor. Once the SUVs were deposited on the Au sensor, the viscoelasticity of the film
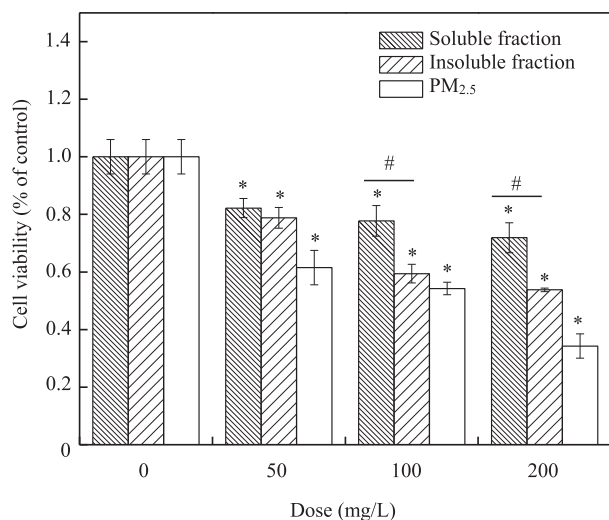

Fig. 3 – Cell viability is detected by the 3-(4,5-dimethylthiazol-2-thiazoyl)-2,5-diphenyl-2-H-tetrazolium bromide (MTT) assay. Cells were exposed to the total PM$_{2.5}$, soluble and insoluble fractions for 24 hr at the concentration of 0, 50, 100, 200 mg/L. The cell viability after PM$_{2.5}$ treatment was calculated as a percentage of control group (0 mg/L) (*) indicates a significant difference ($p < 0.05$) compared to control (#) indicates the significant difference ($p < 0.05$) of the comparison between the soluble and insoluble fractions at the same concentration. Error bars represent standard deviations for three replicates.

on the sensor started to increase. ΔD increased initially and then gradually stabilized after formation of an intact SUV layer.

After the 20 mg/L PM$_{2.5}$ suspension flowed through the negatively charged SUV-layer for 1 hr, Δf decreased approximately 13 Hz and ΔD increased approximately 5×10^{-6} (Fig. 2c). The decrease in Δf was caused by the mass increase on the sensor, which indicated that PM$_{2.5}$ could adhere to the negatively charged SUVs. PM$_{2.5}$ can be transported from its suspension to the membrane surface via particle diffusion. Membrane charge polarization promotes particle attachment on the overall negatively charged membranes (Zhang et al., 2019). For living cells, the membranes are negatively charged but contain relatively fewer cationic domains than anionic domains (Wilke and Maggio, 2011). PM$_{2.5}$ can adhere to cell membranes via these cationic domains and forces other than electrostatic attraction. Therefore, electrostatic repulsion is insufficient to prevent PM$_{2.5}$ from attaching to cell membranes.

For the sake of comparison, a 20 mg/L PM$_{2.5}$ suspension was also injected into the positively charged SUV-layer for 1 hr, and Δf increased quickly at first and then decreased slowly (Fig. 2d), whereby the change in ΔD was opposite to that of Δf, which indicated that PM$_{2.5}$ caused rapid membrane disruption once PM$_{2.5}$ came into contact with the positively charged SUVs. Electrostatic attraction worked together with other intermolecular forces in this process. Al–OH of the kaolinite in PM$_{2.5}$ can react with O–P of phospholipids to form hydrogen bonds (Yuan et al., 1995). In addition, PM$_{2.5}$ adhered to the A549 cells and caused physical membrane damage (Fig. 4b). The quick increase in Δf was due to the removal of disrupted lipid fragments and the mass loss on the QCM

sensor. Later, an increasing amount of PM$_{2.5}$ was electrostatically attracted to the SUVs, which caused a mass increase on the sensor; hence, Δf started to gradually decrease (Fig. 2d). The change in Δf of the positively charged SUV layer was initially governed by SUV breakdown, which was later determined to be caused by PM$_{2.5}$ adhesion.

2.3. Cell viability and membrane integrity detected by MTT and LDH assay

The viability and membrane integrity of the A549 cells were assessed by MTT and LDH assays after treatment with the total PM$_{2.5}$ and insoluble and soluble fractions (Figs. 3 and 4). A significant decrease in cell viability and increase in LDH release were observed compared with the control group, which indicates that PM$_{2.5}$ can cause cell death and cell membrane damage. The cell viability decreased by 27.3%, and the cell membranes were seriously destroyed when exposed to 50 mg/L of total PM$_{2.5}$. Cell viability and membrane integrity decreased as the exposure concentration increased; hence, the total PM$_{2.5}$ and the soluble and insoluble PM$_{2.5}$ fractions all had notable dose effects. The total PM$_{2.5}$ had a more serious influence on cell viability and membrane integrity than the soluble and insoluble PM$_{2.5}$ fractions, and the insoluble PM$_{2.5}$ fraction exerted a more serious influence than the soluble fraction (cell mortality/membrane damage: total PM$_{2.5}$ > insoluble fraction > soluble fraction) (Figs. 3 and 4). On the bright-field images, PM$_{2.5}$ had gathered on the A549 cells but was not uniformly dispersed in the media (Fig. 4b), indicating that PM$_{2.5}$ tended to adhere to cell membranes (Fig. 4b, white arrows). PM$_{2.5}$ adhesion can lead to inhibition of substance exchange and signal transmission into cells. The cell
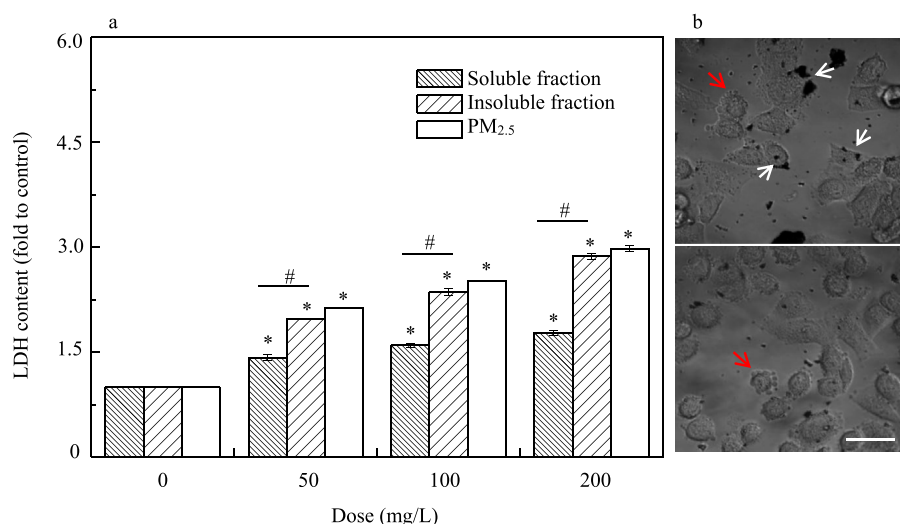

Fig. 4 – (a) Cell membrane integrity is evaluated by lactate dehydrogenase (LDH) assay. Cells were exposed to the total PM$_{2.5}$, soluble and insoluble fractions for 24 hr at the concentration of 0, 50, 100 and 200 mg/L. Date was shown as fold to control (*) indicates significant difference ($p < 0.05$) compared to control (#) indicates a significant difference ($p < 0.05$) of the comparison between the soluble and insoluble fractions at the same concentration; (b) The magnification of the bright field images for cells that are exposed to the total PM$_{2.5}$ at 200 mg/L for 24 hr. Scale bars: 20 μm. White arrow: Cells adhered by PM$_{2.5}$. Red arrow: Cells appeared with small bulbs. Error bars represent standard deviations for three replicates parallel experiments.
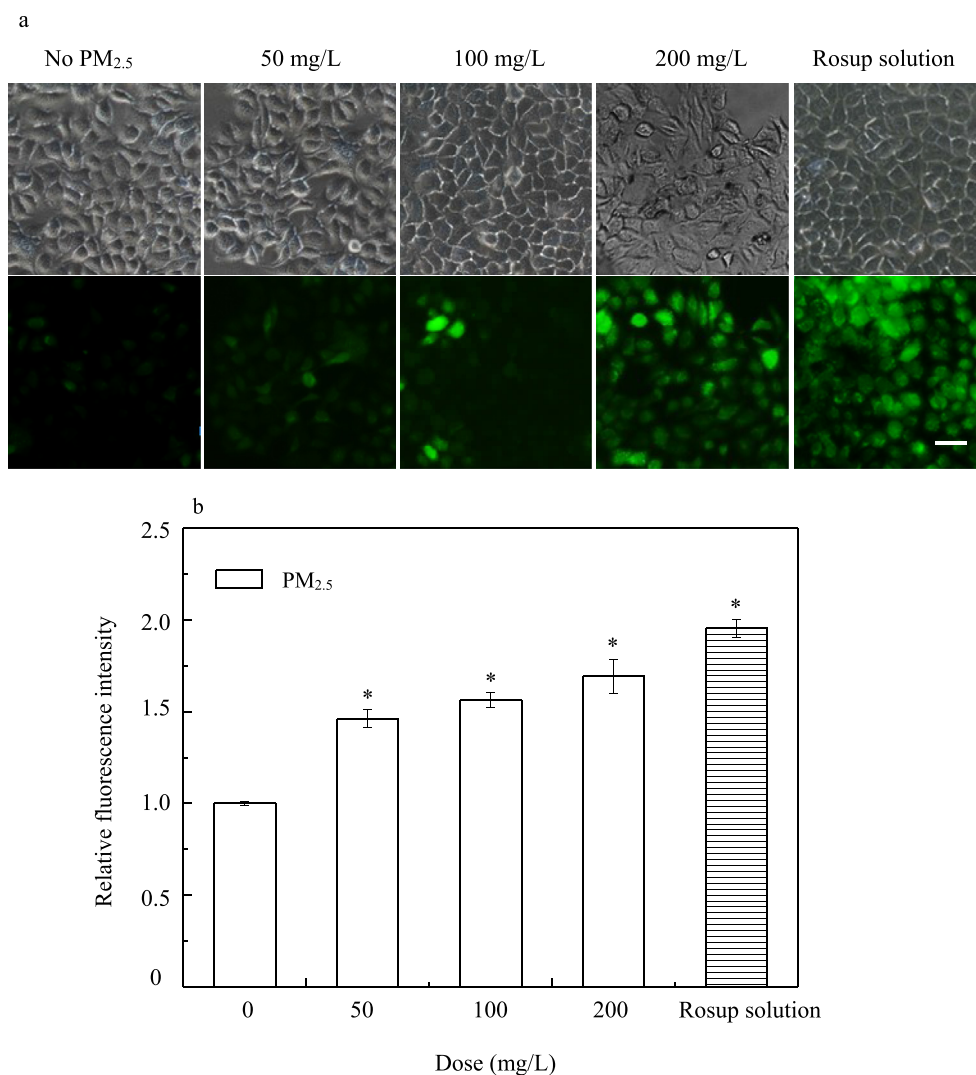
Fig. 5 – (a) The bright field (upper) and fluorescence (lower) images at the same vision scope reveal the cellular reactive oxygen species (ROS) production after the exposure of 0, 50, 100 and 200 mg/L $PM_{2.5}$ for 48 hr; (b) The relative fluorescence intensity represents the ROS level of A549 cells treated with 0, 50, 100 and 200 mg/L $PM_{2.5}$ for 48 hr (*) indicates a significant difference ($p < 0.05$) of the comparison to the control. Scale bars: 20 μm. Error bars represent standard deviations for three replicates.

morphology changed from spindle to irregular shapes and swelling occurred in these cells (Fig. 4b). Small bubbles appeared on the cell surface after exposure to 200 mg/L $PM_{2.5}$ for 24 hr (Fig. 4b, red arrows). Such phenomena might be a sign of cell necrosis, and in this process, pores were formed in the membrane (Chen et al., 2016). Membrane leakage disturbs the ion and water fluxes across the membrane, and intracellular content is released, which causes the cellular swelling and blebbing. Either physical contact with $PM_{2.5}$ or cell necrosis can cause cell membrane rupture.

Soluble $PM_{2.5}$ components easily enter cells and quickly induce early adverse effects. Inorganic ion NO_3^- can induce the abnormal production of cytokines (Huang et al., 2003). The aliphatic carbons, aromatic compounds and quinone moieties

are important factors causing genotoxic effects (Jia et al., 2017). The insoluble fractions were reported to play a significant role in inflammatory and cytotoxic activities and to act as carriers for the soluble fractions (Jalava et al., 2008). The insoluble $PM_{2.5}$ fractions caused a higher cell mortality and more serious cell membrane damage than the soluble $PM_{2.5}$ fraction (Figs. 3 and 4). The insoluble $PM_{2.5}$ fractions, including kaolinite, $CaCO_3$, water-insoluble carbon, aromatic rings, and hydroxyl and carboxyl groups, are suggested to form hydrogen bonds or other short-range intermolecular forces with the phosphate groups on the cell membranes, which leads to particle adhesion and cell membrane damage. Physical and chemical damage to membranes will definitely decrease cell viability. In addition, certain transition metals (such as Fe, Cu, and Mn) existing in the

insoluble fraction are suggested to perform remarkable cytotoxicity (Wang et al., 2013b). Moreover, the insoluble particles that internalized into the cells and localized in laminar organelles were also reported to damage mitochondria and lysosomes (Gualtieri et al., 2011).

2.4. $PM_{2.5}$ can induce cellular ROS production

ROS production in the A549 cells was imaged by fluorescence microscopy. Very weak fluorescence was detected in the 0 mg/L $PM_{2.5}$ solution (Fig. 5a), indicating the minimal ROS production. The fluorescence intensity (ROS production) increased gradually with the $PM_{2.5}$ concentration (0–200 mg/L) (Fig. 5a and b). ROS assays were conducted after exposure to 200 mg/L total $PM_{2.5}$ and the soluble and insoluble $PM_{2.5}$ fractions. According to the fluorescence images and fluorescence quantification, the cells treated with the total $PM_{2.5}$ and the soluble and insoluble $PM_{2.5}$ fractions all exhibited significantly increased fluorescence intensities (Fig. 6a and b). Moreover, the cell morphology changed from spindle to irregular shapes after $PM_{2.5}$ exposure, and cell number also decreased (Fig. 6a).

The components in the soluble $PM_{2.5}$ fraction, including organic acids, NH_4^+, SO_4^{2-}, and NO_3^- ions, carboxyl groups and aromatic compounds (Table 1), can stimulate cells and elevate the ROS level (Ryan et al., 2009). Water-soluble carbon is reported to be a significant source of ROS generation (Zhang et al., 2008). The presence of phenols raises the exogenous ROS level (Khachatryan et al., 2006), and the reactive quinones are responsible for ROS generation (Wang et al., 2013a; Zou et al., 2016). When insoluble particles enter cells via endocytosis, metals (such as Fe, Cu, Mn and Cr) increase the ROS level by disrupting the activity of the involved enzymes (Feng et al., 2016). The iron element can accumulate in lysosomes (Nankivell et al., 1992) and increase ROS production as a byproduct
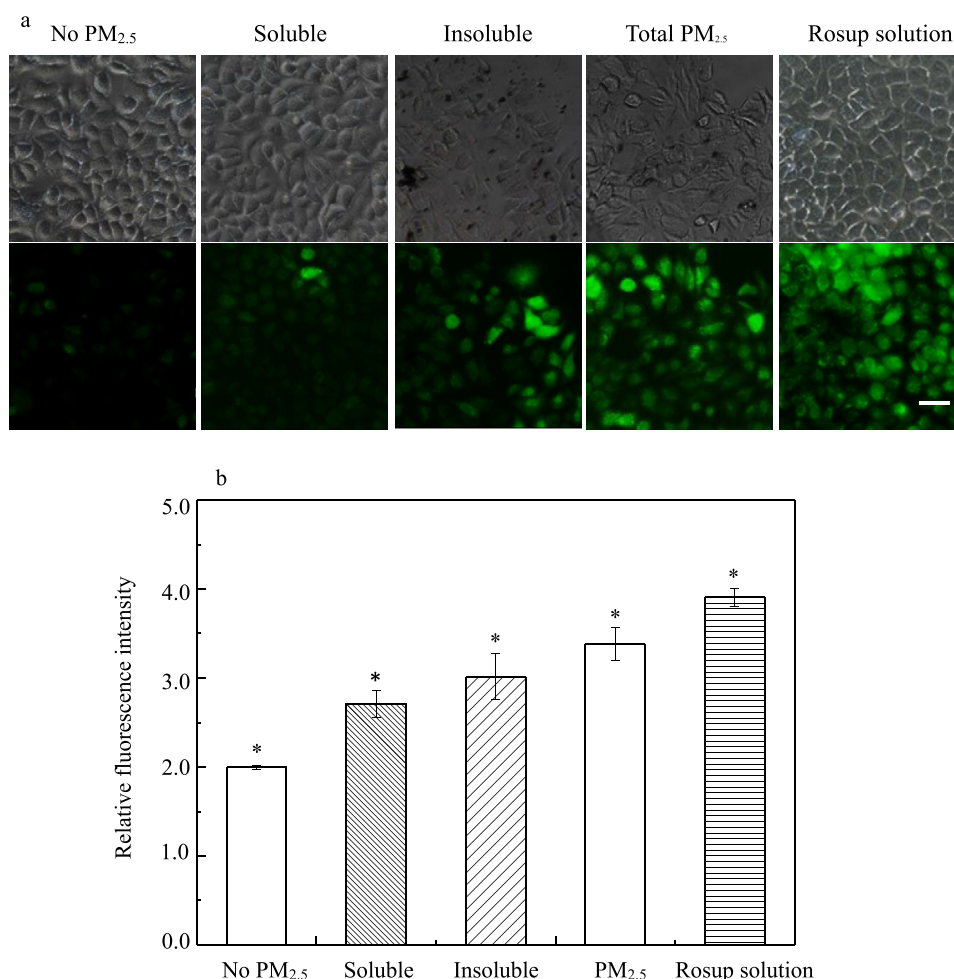

Fig. 6 – (a) The bright field (upper) and fluorescence (lower) images show the cellular ROS level for the treatments of negatively control (No $PM_{2.5}$), 200 mg/L total $PM_{2.5}$, soluble fraction, insoluble fractions and Rosup solution for 48 hr in the same vision; (b) The relative fluorescence intensity represents the ROS level of A549 cells treated with the total $PM_{2.5}$, soluble and insoluble fractions at 200 mg/L for 48 hr (*) indicates a significant difference ($p < 0.05$) of the comparison to the control. Scale bars: 20 μm. Error bars represent standard deviations for three replicates.

in the metabolic process (Zhang et al., 2008). Therefore, the multiple substances in either the soluble or insoluble PM$_{2.5}$ fractions can increase the cellular ROS level. Hence, the cellular ROS level is enhanced by both the soluble and insoluble PM$_{2.5}$ fractions in this study, and the values are not significantly different (Fig. 6a and b).

Decreased cell viability, cell membrane damage and increased ROS production are correlated with toxic effects induced by PM$_{2.5}$. Particle-induced lipid peroxidation has been suggested to be an important mechanism of cell membrane damage (Huang et al., 2003; Karlsson et al., 2005). Excess ROS generation may disrupt the balance of the anti-oxidation system and result in oxidative stress (Laing et al., 2010). ROS can oxidize and inactivate proteins and lipids in the cell membrane and thereby increase membrane permeability and fluidity, which increases the intracellular Ca^{2+} level, damages intracellular calcium homeostasis and decreases cell viability (Geng et al., 2005). Moreover, ROS can attack and inactivate intracellular biomacromolecules, which can lead to apoptosis (Ray et al., 2012). Therefore, we observed that the high PM$_{2.5}$ dose increased the ROS level (Fig. 6a and b), decreased cell viability and induced more serious membrane disruption (Figs. 3 and 4). Oxidative stress can trigger cell membrane damage and cell death.

3. Conclusions

In this study, we analyzed the physicochemical properties of PM$_{2.5}$ collected in Jinan to investigate the effect of PM$_{2.5}$ solubility on its cytotoxicity. We studied the interaction of PM$_{2.5}$ with simulated cell membranes and the exposure to A549 cell lines and compared the differences between the soluble and insoluble PM$_{2.5}$ fractions. PM$_{2.5}$ can adhere to either positively charged or negatively membranes but disrupts the positively charged membranes. Both the soluble and insoluble PM$_{2.5}$ fractions decrease cell viability, destroy cell membrane integrity and stimulate ROS production. However, the insoluble PM$_{2.5}$ fraction induces more serious membrane damage and cell mortality than does the soluble PM$_{2.5}$ fraction. The attachment of solid particles on the membrane surface and the transition metals in the insoluble PM$_{2.5}$ fraction cause this difference. The soluble and insoluble PM$_{2.5}$ fractions cause similar ROS level enhancement. Therefore, the cytotoxicity of PM$_{2.5}$ has a certain relationship with its fractions.

Conflict of interest

The authors declared that they have no conflicts of interest to this work.

Acknowledgments

REFERENCES

Allen, D.T., Palen, E.J., Haimov, M.I., Hering, S.V., Young, J.R., 1994. Fourier transform infrared spectroscopy of aerosol collected in a low pressure impactor (LPI/FTIR): method development and field calibration. Aerosol Sci. Technol. 21 (4), 325–342.

Anil, I., Golcuk, K., Karaca, F., 2014. ATR-FTIR spectroscopic study of functional groups in aerosols: the contribution of a saharan dust transport to urban atmosphere in istanbul, Turkey. Water Air Soil Pollut 225 (3), 1898.

Block, M.L., Calderón-Garcidueñas, L., 2009. Air pollution: mechanisms of neuroinflammation and CNS disease. Trends Neurosci 32, 506–516.

Calderón-Garcidueñas, L., Solt, A.C., Henríquez-Roldán, C., Torres-Jardón, R., Nuse, B., Herritt, L., et al., 2008. Long-term air pollution exposure is associated with neuroinflammation, an altered innate immune response, disruption of the blood-brain barrier, ultrafine particulate deposition, and accumulation of amyloid β-42 and α-synuclein in children and young adults. Toxicol. Pathol. 36 (2), 289–310.

Cao, C., Jiang, W., Wang, B., Fang, J., Lang, J., Tian, G., et al., 2014. Inhalable microorganisms in Beijing's PM$_{2.5}$ and PM$_{10}$ pollutants during a severe smog event. Environ. Sci. Technol. 48 (3), 1499–1507.

Chen, X., He, W.T., Hu, L., Li, J., Fang, Y., Wang, X., et al., 2016. Pyroptosis is driven by non-selective gasdermin-D pore and its morphology is different from MLKL channel-mediated necroptosis. Cell Res 26, 1007–1020.

Cho, N., Frank, C.W., Kasemo, B., Hook, F., 2010. Quartz crystal microbalance with dissipation monitoring of supported lipid bilayers on various substrates. Nat. Protoc. 5 (6), 1096–1106.

Deng, X., Zhang, F., Rui, W., Long, F., Wang, L., Feng, Z., et al., 2013. PM2.5-induced oxidative stress triggers autophagy in human lung epithelial A549 cells. Toxicol. In Vitro 27 (6), 1762–1770.

Duarte, R.M.B.O., Pio, C.A., Duarte, A.C., 2004. Synchronous scan and excitation-emission matrix fluorescence spectroscopy of water-soluble organic compounds in atmospheric aerosols. J. Atmos. Chem. 48 (2), 157–171.

Duarte, R.M.B.O., Santos, E.B.H., Pio, C.A., Duarte, A.C., 2007. Comparison of structural features of water-soluble organic matter from atmospheric aerosols with those of aquatic humic substances. Atmos. Environ. 41 (37), 8100–8113.

Feng, S., Gao, D., Liao, F., Zhou, F., Wang, X., 2016. The health effects of ambient PM$_{2.5}$ and potential mechanisms. Ecotox. Environ. Safe. 128, 67–74.

Geng, H., Meng, Z., Zhang, Q., 2005. Effects of blowing sand fine particles on plasma membrane permeability and fluidity, and intracellular calcium levels of rat alveolar macrophages. Toxicol. Lett. 157 (2), 129–137.

Geng, H., Meng, Z., Zhang, Q., 2006. In vitro responses of rat alveolar macrophages to particle suspensions and water-soluble components of dust storm PM$_{2.5}$. Toxicol. in Vitro 20 (5), 575–584.

Graber, E.R., Rudich, Y., 2006. Atmospheric HULIS: how humic-like are they? a comprehensive and critical review. Atmos. Chem. Phys. 6 (3), 729–753.

Gualtieri, M., Mantecca, P., Corvaja, V., Longhin, E., Perrone, M.G., Bolzacchini, E., et al., 2009. Winter fine particulate matter from Milan induces morphological and functional alterations in human pulmonary epithelial cells (A549). Toxicol. Lett. 188 (1), 52–62.

Gualtieri, M., Øvrevik, J., Mollerup, S., Asare, N., Longhin, E., Dahlman, H., et al., 2011. Airborne urban particles (Milan winter-PM$_{2.5}$) cause mitotic arrest and cell death: effects on

DNA, mitochondria, AhR binding and spindle organization. Mutat. Res. 713 (1–2), 18–31.

Huang, S.L., Hsu, M.K., Chan, C.C., 2003. Effects of submicrometer particle compositions on cytokine production and lipid peroxidation of human bronchial epithelial cells. Environ. Health Perspect. 111 (4), 478–482.

Indo, H.P., Davidson, M., Yen, H., Suenaga, S., Tomita, K., Nishii, T., et al., 2007. Evidence of ROS generation by mitochondria in cells with impaired electron transport chain and mitochondrial DNA damage. Mitochondrion 7 (1–2), 106–118.

Jalava, P.I., Salonen, R.O., Pennanen, A.S., Happo, M.S., Penttinen, P., Hälinen, A.I., et al., 2008. Effects of solubility of urban air fine and coarse particles on cytotoxic and inflammatory responses in RAW 264.7 macrophage cell line. Toxicol. Appl. Pharmacol. 229 (2), 146–160.

Jia, Y., Wang, Q., Liu, T., 2017. Toxicity research of PM$_{2.5}$ compositions in vitro. Int. J. Environ. Res. Public Health. 14 (3), 232.

Kampa, M., Castanas, E., 2008. Human health effects of air pollution. Environ. Pollut. 151, 362–367.

Karlsson, H.L., Nilsson, L., Möller, L., 2005. Subway Particles are more genotoxic than street particles and induce oxidative stress in cultured human lung cells. Chem. Res. Toxicol. 18 (1), 19–23.

Karthikeyan, S., Balasubramanian, R., 2006. Determination of water-soluble inorganic and organic species in atmospheric fine particulate matter. Microchem J 82 (1), 49–55.

Keller, C.A., Kasemo, B., 1998. Surface specific kinetics of lipid vesicle adsorption measured with a quartz crystal microbalance. Biophys. J. 75, 1397–1402.

Khachatryan, L., Adounkpe, J., Maskos, Z., Dellinger, B., 2006. Formation of cyclopentadienyl radical from the gas-phase pyrolysis of hydroquinone, catechol, and phenol. Environ. Sci. Technol. 40 (16), 5071–5076.

Kioumourtzoglou, M., Schwartz, J.D., Weisskopf, M.G., Melly, S.J., Wang, Y., Dominici, F., et al., 2016. Long-term PM$_{2.5}$ exposure and neurological hospital admissions in the northeastern united states. Environ. Health Perspect. 124 (1), 23–29.

Klapper, L., McKnight, D.M., Fulton, J.R., Blunt-Harris, E.L., Nevin, K.P., Lovley, D.R., et al., 2002. Fulvic acid oxidation state detection using fluorescence spectroscopy. Environ. Sci. Technol. 36 (14), 3170–3175.

Laing, S., Wang, G., Briazova, T., Zhang, C., Wang, A., Zheng, Z., et al., 2010. Airborne particulate matter selectively activates endoplasmic reticulum stress response in the lung and liver tissues. Am. J. Physiol.-Cell Physiol. 299 (4), 736–749.

Leenheer, J.A., Croué, J.P., 2003. Characterizing aquatic dissolved organic matter. Environ. Sci. Technol. 37, 18A–26A.

Ma, Y., Cheng, Y., Qiu, X., Cao, G., Fang, Y., Wang, J., et al., 2018. Sources and oxidative potential of water-soluble humic-like substances (HULISWS) in fine particulate matter (PM$_{2.5}$) in Beijing. Atmos. Chem. Phys 18, 5607–5617.

Maria, S.F., Russell, L.M., Turpin, B.J., Porcja, R.J., 2002. FTIR measurements of functional groups and organic mass in aerosol samples over the Caribbean. Atmos. Environ. 36 (33), 5185–5196.

Nankivell, B.J., Boadle, R.A., Harris, D.C.H., 1992. Iron accumulation in human chronic renal disease. Am. J. Kidney Dis. 20 (6), 580–584.

Nie, W., Wang, T., Gao, X., Pathak, R.K., Wang, X., Gao, R., et al., 2010. Comparison among filter-based, impactor-based and continuous techniques for measuring atmospheric fine sulfate and nitrate. Atmos. Environ. 44 (35), 4396–4403.

Ofner, J., Krüger, H.U., Grothe, H., Schmitt-Kopplin, P., Whitmore, K., Zetzsch, C., 2011. Physico-chemical characterization of SOA derived from catechol and guaiacol-a

model substance for the aromatic fraction of atmospheric HULIS. Atmos. Chem. Phys. 10 (7), 17369–17405.

Panteliadis, P., Hafkenscheid, T., Cary, B., Diapouli, E., Fischer, A., Favez, O., et al., 2015. Ecoc comparison exercise with identical thermal protocols after temperature offset correction-instrument diagnostics by in-depth evaluation of operational parameters. Atmos Meas Tech 8 (2), 779–792.

Ravisankar, R., Kiruba, S., Eswaran, P., Senthilkumar, G., Chandrasekaran, A., 2010. Mineralogical characterization studies of ancient potteries of tamilnadu, India by FT-IR spectroscopic technique. E-J Chem 7 (1), 185–190.

Ray, P., Huang, B.W., Tsuji, Y., 2012. Reactive oxygen species (ROS) homeostasis and redox regulation in cellular signaling. Cell. Signal. 24 (5), 981–990.

Rodahl, M., Höök, F., Fredriksson, C., Keller, C.A., Krozer, A., Brzezinski, P., et al., 1997. Simultaneous frequency and dissipation factor QCM measurements of biomolecular adsorption and cell adhesion. Faraday Discuss 107, 229–246.

Ryan, P.H., Bernstein, D.I., Lockey, J., Reponen, T., Levin, L., Grinshpun, S., et al., 2009. Exposure to traffic-related particles and endotoxin during infancy is associated with wheezing at age 3 years. Am. J. Respir. Crit. Care Med. 180 (11), 1068–1075.

Shaka, H., Saliba, N.A., 2004. Concentration measurements and chemical composition of PM$_{10-2.5}$ and PM$_{2.5}$ at a coastal site in Beirut, Lebanon. Atmos. Environ. 38 (4), 523–531.

Soukup, J.M., Becker, S., 2001. Human alveolar macrophage responses to air pollution particulates are associated with insoluble components of coarse material, including particulate endotoxin. Toxicol. Appl. Pharmacol. 171 (1), 20–26.

Thron, R.W., 1996. Direct and indirect exposure to air pollution. Otolaryng Head Neck 114 (2), 281–285.

Valavanidis, A., Fiotakis, K., Vlachogianni, T., 2008. Airborne particulate matter and human health: toxicological assessment and importance of size and composition of particles for oxidative damage and carcinogenic mechanisms. J. Environ. Sci. Health 26 (4), 339–362.

Voliotis, A., Prokeš, R., Lammel, G., Samara, C., 2017. New insights on humic-like substances associated with wintertime urban aerosols from central and southern Europe: size-resolved chemical characterization and optical properties. Atmos. Environ. 166, 286–299.

Vuong, N.Q., Breznan, D., Goegan, P., O'Brien, J.S., Williams, A., Karthikeyan, S., et al., 2017. In vitro toxicoproteomic analysis of A549 human lung epithelial cells exposed to urban air particulate matter and its water-soluble and insoluble fractions. Part. Fibre Toxicol 14 (1), 39.

Wang, B., Li, K., Jin, W., Lu, Y., Zhang, Y., Shen, G., et al., 2013a. Properties and inflammatory effects of various size fractions of ambient particulate matter from Beijing on A549 and J774A.1 Cells. Environ. Sci. Technol. 47 (18), 10583–10590.

Wang, D., Pakbin, P., Shafer, M.M., Antkiewicz, D., Schauer, J.J., Sioutas, C., 2013b. Macrophage reactive oxygen species activity of water-soluble and water-insoluble fractions of ambient coarse, PM$_{2.5}$ and ultrafine particulate matter (PM) in Los Angeles. Atmos. Environ. 77, 301–310.

Wilke, N., Maggio, B., 2011. Electrostatic field effects on membrane domain segregation and on lateral diffusion. Biophys. Rev. 3 (4), 185–192.

Yousefi, N., Tufenkji, N., 2016. Probing the interaction between nanoparticles and lipid membranes by quartz crystal microbalance with dissipation monitoring. Front. Chem. 4, 46.

Yan, Z., Wang, J., Li, J., Jiang, N., Zhang, R., Yang, W., et al., 2016. Oxidative stress and endocytosis are involved in upregulation of interleukin-8 expression in airway cells exposed to PM$_{2.5}$. Environ. Toxicol. 31 (12), 1869–1878.

Yuan, C., Zhao, D., Liu, A., Ni, J., 1995. A NMR study of the interaction of silica with dipalmitoylphosphatidylcholine liposomes. J. Colloid Interface Sci. 172 (2), 536–538.

Zhang, H., Wei, X., Liu, L., Zhang, Q., Jiang, W., 2019. The role of positively charged sites in the interaction between model cell membranes and γ-Fe$_2$O$_3$ NPs. Sci. Total Environ. 673, 414–423.

Zhang, Y., Schauer, J.J., Shafer, M.M., Hannigan, M.P., Dutton, S.J., 2008. Source apportionment of in vitro reactive oxygen species bioassay activity from atmospheric particulate matter. Environ. Sci. Technol. 42 (19), 7502–7509.

Zhang, Y., Li, Y., Shi, Z., Wu, J., Yang, X., Feng, L., et al., 2018. Metabolic impact induced by total, water soluble and insoluble components of PM$_{2.5}$ acute exposure in mice. Chemosphere 207, 337–346.

Zhou, Q., Wang, L., Cao, Z., Zhou, X., Yang, F., Fu, P., et al., 2016. Dispersion of atmospheric fine particulate matters in simulated lung fluid and their effects on model cell membranes. Sci. Total Environ. 542, 36–43.

Zhu, Y., Olson, N., Beebe, T.P., 2001. Surface chemical characterization of 2.5-μmp articulates (PM$_{2.5}$) from air pollution in Salt Lake City using TOF-SIMS, XPS, and FTIR. Environ. Sci. Technol. 35 (15), 3113–3121.

Zhuang, X., Wang, Y., He, H., Liu, J., Wang, X., Zhu, T., et al., 2014. Haze insights and mitigation in China: an overview. J. Environ. Sci. 26, 2–12.

Zou, Y., Jin, C., Su, Y., Li, J., Zhu, B., 2016. Water soluble and insoluble components of urban PM2.5 and their cytotoxic effects on epithelial cells (A549) in vitro. Environ. Pollut. 212, 627–635.